Viscosity and friction pressure measurements of fiber suspensions

Victor Nogueira Lima[1], Erlend Randeberg[2], Hans Joakim Skadsem[2,3], Flávio de Andrade Silva[1]
[1]Pontifícia Universidade Católica do Rio de Janeiro (PUC-Rio), Rio de Janeiro, Brazil
[2]NORCE Norwegian Research Centre AS, Stavanger, Norway
[3]University of Stavanger, Stavanger, Norway

ABSTRACT

Fiber additions can improve the performance of well construction fluids, such as drilling fluids and completion fluids, by reducing fluid loss to permeable formations and improving hole cleaning. Fibers can also impart ductility to hardened cements, and improve its resistance to tensile crack propagation. Polyvinyl alcohol (PVA) fibers have been identified as an interesting addition for well cement slurries, but its impact on the rheological properties of the suspension has not been studied before. To this end, we study the viscosity and friction pressure of Newtonian and non-Newtonian fiber suspensions with increasing concentration of PVA fibers. We report viscosity measurements of the suspensions using an eight-speed viscometer equipped with a narrow gap and a wide gap Couette geometry, and fit measurements to constitutive viscosity models. Subsequently, friction pressure measurements for the fiber suspensions are acquired from a pipe flow loop and compared to predictions based on the viscosity characterization. We find a small viscosifying effect of increasing fiber concentrations. Friction pressure measurements for the non-Newtonian fiber suspension are in excellent agreement with theoretical predictions for generalized Reynolds numbers over three orders of magnitude.

INTRODUCTION

The rheology of fiber suspensions is of great importance for the paper-making industry and for the production of fiber reinforced polymeric materials. Fibers are also routinely used as additives in well construction fluids to improve hole cleaning and to reduce fluid loss to permeable formations. As the shape of fiber particles is often rod-like, with a high length to diameter ratio, fiber particle interaction and flocculation become prominent at low fiber concentrations. Indeed, concentrations of less than 0.1% of high-aspect ratio fibers have been found highly effective in improving hole cleaning in deviated wellbores due to the formation of a fiber mat network in the suspending fluid.[1]

For effective application of fibers in well construction fluids, it is important to understand how fiber additives affect the rheological behavior of the suspension, and whether fiber particles flocculate or remain dispersed. Previous work focusing on the impact of fibers on rheological properties has found that the concentration and shape of fiber particles affect both the viscosity of the suspension[2,3] and also the velocity profile and the

particle distribution in Poiseuille flow.[4,5] Similar to shear-induced migration of spherical particles,[6] fiber particles tend to concentrate in regions of low shear rate in Poiseuille flow,[4] *i.e.* toward the center of the duct. When sheared between parallel plates, recent research has shown that flexible fiber particles migrate toward the center of the gap.[7] Thus, the local fiber concentration is likely lower adjacent to bounding walls, and this local depletion may impact *e.g.* viscosity measurement through an apparent wall slip. Further, as the length of common fiber particles is often similar to the gap width in conventional cylindrical Couette viscometers, the measurement geometry may also constrain the fiber particle orientation to a near-parallel alignment with the walls. Constraining the fiber orientation is considered to reduce the viscosity compared to a fiber suspension with random particle orientations.[5]

The present study focuses on the impact of different concentrations of polyvinyl alcohol (PVA) fibers on the viscosity and friction pressure of a Newtonian and a non-Newtonian suspending fluid. This type of fiber has been shown to enhance the performance of hardened well cement,[8] but its impact on rheological properties is still unexplored. In preparation of tests with actual cement systems, we report results acquired with model non-hardening fluids with different concentrations PVA. We measure the fiber suspension viscosity using both a narrow gap and a wide gap viscometer geometry to probe any gap width dependency on the viscosity. The results are then compared to measurements of laminar friction pressure when the fiber suspensions are circulated through a pipe.

EQUIPMENT AND METHODS

We study fiber influence on viscosity and friction pressure gradient in a Newtonian fluid and in a polymeric, shear thinning fluid. The Newtonian fluid was prepared by mixing glycerol and tap water at a fraction of 9:1 by volume. The xanthan gum solution was mixed by adding concentrated, liquid xanthan gum to water to achieve a 3% volume fraction of liquid xanthan gum. As fiber addition, we have studied different volume fractions of Kuralon RMS702 PVA fibers, manufactured by Kuraray. The nominal length of the fibers is 6 mm, and the nominal diameter is 27 µm, producing a considerable aspect ratio of approximately 222. The fiber contents used in our study were 0.25% and 0.5%, which is in the semi-dilute to concentrated fiber suspension regime.[2] Although xanthan gum solutions are normally considered shear thinning fluids, we anticipate that increasing fiber concentrations can promote yield stress behavior in the fiber suspension. To this end, we will base the analysis below on the Herschel-Bulkley model, $\eta(\dot{\gamma}) = \tau_y/\dot{\gamma} + K\dot{\gamma}^{n-1}$, where $\eta = \tau/\dot{\gamma}$ is the shear date-dependent viscosity of the fluid, and τ and $\dot{\gamma}$ denote the shear stress and the shear rate, respectively. Further, τ_y, K and n are yield stress, consistency index and the flow behavior index, respectively.

Viscometer

A Fann 35 oilfield viscometer has been used to measure the viscosity of all suspensions. The viscometer consists of a rotating, outer cylinder and a static inner bob that is attached to a torsional spring (F1), and that enables measurement of the torque on the bob. The most common rotor-stator combination for this viscometer is denoted R1-B1, consisting of a stator (B1) with radius $a = 17.245$ mm and rotor (R1) with radius $b = 18.415$ mm. This combination produces a narrow measurement gap of 1.17 mm. While the R1-B1 geometry is suitable for most conventional well construction fluids, such as drilling fluids and cement

slurries, the relatively narrow gap may restrict the orientation of the slender PVA fibers utilized in this study. Consequently, we have also utilized a wide gap geometry where the standard stator (B1) is exchanged with a smaller stator (B2) of radius of $a = 12.276$ mm. The resulting R1-B2 geometry produces a measurement gap width of 6.139 mm, which is similar to the nominal fiber length. We note that the fiber orientation may still be restricted, even if the gap is now larger than the nominal fiber length. Further details for the measurement geometry is sketched in Fig. 1a. The B1 and B2 stators both have a flat bottom surface, a measurement gap of height $h = 38$ mm, and a coned top surface that makes an angle 30° to the horizontal direction.

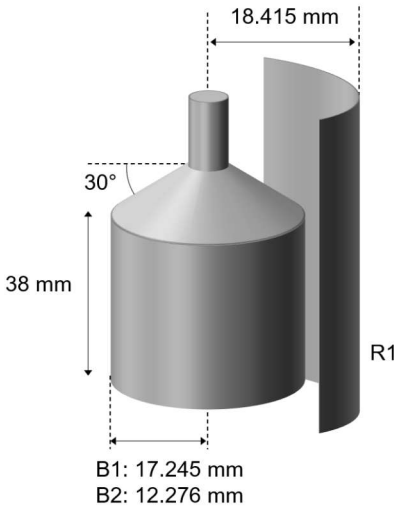

(a) Dimensions of the R1-B2 measurement geometry.

(b) Fluid tank and progressive cavity pump

FIGURE 1: The Fann 35 viscometer with the R1-B2 wide gap measurement cell is used for characterizing the non-Newtonian fiber suspensions.

Non-Newtonian corrections to shear stress and shear rate

The viscometer used in this study to characterize fiber suspension viscosity is a direct reading apparatus, where the torque on the stator is measured at different, fixed angular velocities of the outer cylinder. Conventional conversion factors for converting the torque and the angular velocity to corresponding shear stress and shear rate at the wall of the bob are normally based on the assumption that the test liquid is *Newtonian*. As discussed by *e.g.* Lac and Parry[9] and Skadsem and Saasen,[10] the conventional conversion factors are not always suitable for non-Newtonian test liquids, since now the shear rate in the gap and the stress over the ends of the stator both depend on the liquid viscosity. Specifically, the measured torque T is due to the wall shear stress acting over the submerged surfaces of the stator, *i.e.* over the main cylindrical body, the flat bottom surface and the coned top surface (neglecting the topmost, thin shaft), as illustrated in Fig. 1a. Now, T is normally converted to an equivalent wall shear stress τ_w acting over the cylindrical part of the stator as $\tau_w = T/(2\pi a^2 h)(1+\varphi)^{-1}$, where φ is a numerical correction factor that accounts for the end effects, *i.e.* the shear stress acting over the bottom flat surface and over the coned top surface. A factor of $\varphi = 0.064$ is normally assumed for the standard R1-B1

measurement geometry.[9] As shown by Lac and Parry in their computational study, φ will generally also depend on the flow behavior index, n, and on a Couette-Bingham number, $B = \tau_y/(K\Omega^n)$, with Ω the angular velocity of the rotor. For the current study, we use the geometry-dependent fitting functions for $\varphi(n, B)$ as provided in the supplementary material to Ref. 9.

The second consideration when testing non-Newtonian liquids in viscometers is the determination of the true wall shear rate. When sheared in the gap, the wall shear rate at the stator is to be determined by the velocity profile of the liquid. For Newtonian fluids, the wall shear rate is simply determined by Ω and the aspect ratio $\kappa = a/b$, *i.e.* $\dot{\gamma}_{wN} = 2\Omega/(1-\kappa^2)$. For non-Newtonian fluids, the gap-wise velocity profile depends on the viscosity of the fluid. Thus, the actual wall shear rate is, as per the end correction discussed above, unknown at the time of measurement. In the following, we have corrected the wall shear rate by assuming *a priori* that the test liquids are Herschel-Bulkley fluids, and calculate the non-Newtonian wall shear rates according to Ref. 10.

The two non-Newtonian corrections described above make the problem of identifying the flow curve non-trivial. In this study, we utilize the Levenberg-Marquardt algorithm to iteratively search for the Herschel-Bulkley parameter combination that minimizes the residual sum of squares of the shear stress. The algorithm is initialized with a first guess for each of the model parameters, which in turn are used to convert T and Ω to shear stress and shear rate, as described above. The algorithm next uses the Gauss-Newton and gradient descent methods to obtain improved model parameter values that reduce the residual sum of squares. This procedure is repeated until convergence.

Pipe flow loop

For friction pressure measurements of the fiber suspensions, a flow loop consisting of a pipe test section of $D = 21$ mm inner diameter has been used. A progressive cavity pump, shown in Fig. 1b, has been used to produce flow with no measurable pulsing effects. The friction pressure has been measured using sensors with a measurement range up to 1300 millibar. The two pressure sensors are spaced 150 cm apart, and the first sensor is positioned 70 cm downstream of the pump to allow flow development. A total volume of 17 liter of fiber suspension has been prepared for each test. Samples for viscosity characterization have been collected from the mixing tank connected to the pump.

For fully developed axial flow, the shear stress at the pipe wall, τ_w, is linked to the pressure gradient, $\partial p/\partial z$, as follows: $\tau_w = (\partial p/\partial z)D/4$. The Darcy friction factor, $f = 8\tau_w/(\rho V^2)$ with ρ the fluid mass density and V the bulk velocity, is convenient for hydraulic analyses, since $f = 64/\mathrm{Re}$ in laminar flow of Newtonian fluids. Here, $\mathrm{Re} = \rho V D/\mu$ the Newtonian Reynolds number for pipe flow. When considering non-Newtonian fluids, a *generalized* Reynolds number is introduced, Re_g, that produces the same expression for f in the laminar regime, *i.e.* $f = 64/\mathrm{Re}_g$. As shown by Madlener *et al.*,[11] the generalized Reynolds number for a Herschel-Bulkley fluid is:

$$\mathrm{Re}_g = \frac{8\rho V^2}{\tau_y + K\left(\frac{3m+1}{4m}\dot{\gamma}_{wN}\right)^n}, \tag{1}$$

with $\dot{\gamma}_{wN} = 8V/D$ equal to the Newtonian wall shear rate, and $m = nK\dot{\gamma}_{wN}^n/(\tau_y + K\dot{\gamma}_{wN}^n)$. Thus, if the actual and the predicted friction pressure gradients are in agreement, the measurements should fall on a single $f = 64/\mathrm{Re}_g$ curve, where now Re_g is calculated using the flow curves measured with the viscometer.

Considering the first sensor being 70 cm downstream of the pump, we use the power law correlation developed by Poole and Ridley[12] as guide for development length for having fully developed flow. That is, we assume $X_D/D \approx 0.0567\mathrm{Re}_g$ is a reasonable approximation for the ratio of development length, X_D, to inner pipe diameter at $\mathrm{Re}_g \gtrapprox 100$. As this correlation was developed for power law fluids, Re_g is as per Eq. (1), but with $\tau_y \to 0$. Although the fiber suspensions to be studied in this work may develop yield stress behavior, we assume the correlation still provides a reasonable approximation for the development length. Setting $X_D = 70$ cm, we require $\mathrm{Re}_g \lessapprox 588$ to have fully developed flow throughout the measurement section. Most of the tests reported below satisfy this criterion, although we will also investigate even higher Reynolds number flows.

VISCOSITY CHARACTERIZATION

We consider in Fig. 2 the flow curves for the xanthan gum solutions in the absence of fiber particles, and compare the narrow gap (R1-B1) and the wide gap (R1-B2) geometries. The open symbols correspond to the conventional conversion factors for torque (or dial reading) and rotational speed to respectively shear stress and shear rate. The filled symbols correspond to the non-Newtonian conversion strategy, as explained above. The measurements suggest a highly shear thinning fluid that may, in fact, exhibit a yield

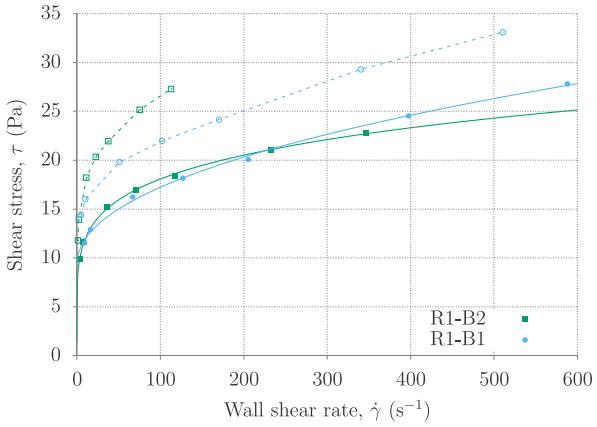

FIGURE 2: Comparison of viscosity measurements of 3% liquid xanthan gum using R1-B1 and R1-B2 measurement geometries. The open symbols correspond to conventional conversion factors for torque and rotational speed. The filled symbols correspond to the non-Newtonian (Herschel-Bulkley) conversion to shear stress and shear rate.

stress (even if xanthan gum solutions are normally considered shear thinning with no yield stress). Further, since the xanthan gum solution does not contain fiber particles, we expect no geometry effects in the properly corrected flow curves. Interestingly, we observe a considerable difference between the R1-B1 and R1-B2 flow curves when considering the conventional conversion factors (open symbols, dashed lines), with the R1-B2 showing consistently higher effective viscosity compared to R1-B1. After performing the non-Newtonian end effect and shear rate corrections, however, we observe a much better agreement across the geometries (filled symbols, solid lines). As seen in the figure, the corrections result in larger shear rates and smaller shear stresses compared to the conventional conversion factors at a given rotational speed and dial reading. Although the fitted Herschel-Bulkley models, shown here as solid lines, deviate at large shear rates, the

measurements (after correction) are found to be in good agreement. Finally, the wide gap geometry (R1-B2) involves larger magnitude corrections, both in terms of shear stress and shear rate. We link this observation to the shear stress variation with radial position, r, in the measurement geometry, *viz.* $\tau \sim r^{-2}$, which results in larger stress variations when measuring with R1-B2 compared to R1-B1. Thus, accounting for non-Newtonian effects are increasingly more important for highly non-Newtonian fluids, but also within wider concentric cylinder geometries.

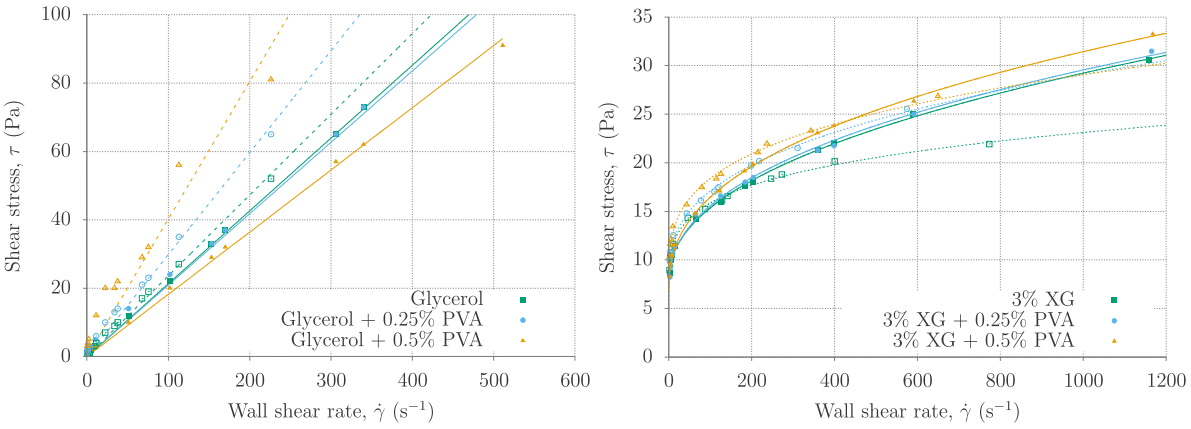

(a) Glycerol as base fluid

(b) Xanthan gum as base fluid

FIGURE 3: Fann 35 measurements using R1-B1 (filled symbols) and R1-B2 (open symbols) measurement geometries. All measurements have been corrected for non-Newtonian shear rates and end effects.

In Fig. 3, we plot flow curves for glycerol (a) and xanthan gum (b), with different concentrations of PVA fiber. Now only data points with the non-Newtonian corrections are shown, and filled symbols correspond to R1-B1 measurement geometry and open symbols to R1-B2. We first note that addition of fiber to glycerol appears to retain the Newtonian characteristic of the suspending liquid; consequently, we have used the conventional (Newtonian) conversion factors when correlating T and Ω to shear stress and shear rate in Fig. 3a. Focusing first on measurements from R1-B1, we observe practically no viscosifying effect of fibers at 0.25% concentration. Surprisingly, the viscosity in fact decreases when the fiber content is increased to 0.5% concentration. For R1-B2, shown by the open symbols, we observe the opposite trend, *i.e.* a consistent increase in viscosity with increasing fiber concentration. The flow curves in Fig. 3b for xanthan gum solutions exhibit pronounced shear thinning and behavior indicative of non-zero yield stress. For both R1-B1 and R1-B2 geometries, we observe a slight tendency for higher effective viscosities as the fiber concentration increases, although the effect is generally small. Surprisingly, the xanthan gum solution with no fibers, as measured in the R1-B2 geometry (open squares), produces a flow curve that is significantly lower than the other measurements at shear rates above approximately 300 s^{-1}.

FRICTION PRESSURE LOSS MEASUREMENTS

Measurements of friction pressure when circulating glycerol and xanthan gum fiber solutions have been converted to the Darcy friction factor f, and are compared to the theoretical result $f = 64/\mathrm{Re}_g$ in Fig. 4, with Re_g given in Eq. (1). In all cases, the viscometer measurements in Fig. 3 are used to calculate the generalized Reynolds number

at a given flow rate. We observe from Fig. 4a that it is generally the viscosity obtained from the narrow gap geometry (R1-B1, filled symbols) that produce the better agreement for glycerol solutions. Good agreement is observed up to 0.25% PVA for Reynolds numbers from about 20 and up to approximately 200. We recall from Fig. 3a that the highest fiber concentration resulted in an apparent drop in viscosity when measured with the narrow gap geometry. When comparing to the theoretical friction factor curve, the

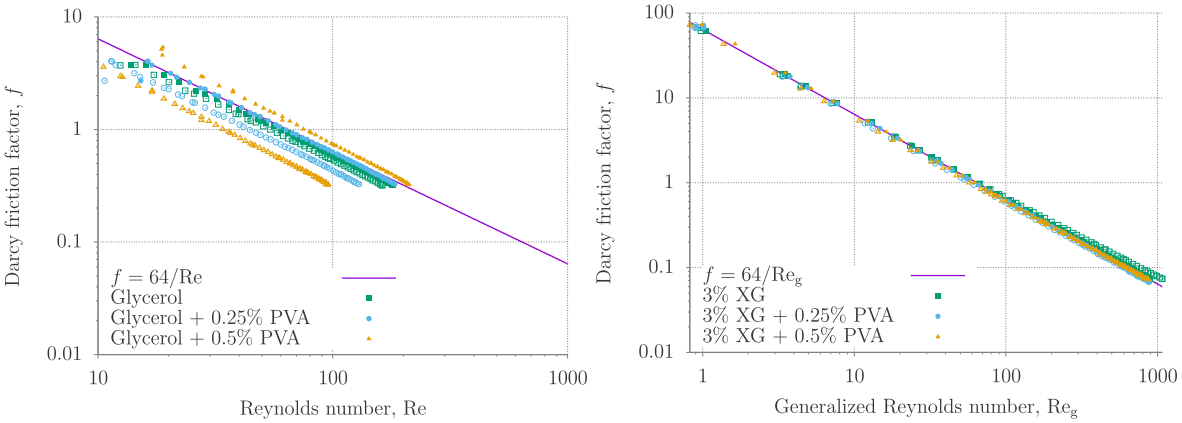

(a) Glycerol as base fluid

(b) Xanthan gum as base fluid

FIGURE 4: Darcy friction factor for laminar pipe flow for the glycerol solutions (a) and the xanthan gum solutions (b). The Reynolds numbers are based on the Fann 35 measurements with either the R1-B1 geometry (filled symbols) or the R1-B2 geometry (open symbols).

Reynolds number appears to be overestimated for measurements with 0.5% PVA fiber. The opposite trend is observed when basing the Reynolds number on the wide gap (R1-B2) viscometer measurements; in Fig. 3a a gradual increase in viscosity was observed with increasing fiber concentration. The friction pressure measurements in Fig. 4a suggest that the corresponding Reynolds numbers are under-estimated. The measurements taken with the different xanthan gum solutions shown in Fig. 4b are in good agreement with the theoretical prediction over the full range of Reynolds numbers considered. We observe a slight deviating trend at the highest Reynolds numbers for the xanthan gum solutions without fibers when basing the generalized Reynolds number on the wide gap (R1-B2) viscometer measurements. The deviation is considered linked to the lower effective viscosity for this sample in Fig. 3b, particularly at high shear rates. Finally, we recall that the criterion for fully developed flow at the first pressure sensor was estimated to $\mathrm{Re}_g < 588$. The agreement between measured and predicted friction factor for Re_g up to 1000 suggests that at least the friction pressure gradient has been largely developed up to the first pressure transmitter.

CONCLUSION

Our study has shown that increasing concentrations of polyvinyl alcohol (PVA) fibers result in a slight increase in the viscosity of the suspension when measured with the narrow gap geometry, and a larger increase when testing the fiber suspension with a Newtonian suspending liquid in the wide gap geometry. Non-Newtonian corrections for shear stress end-effects on the stator and for the wall shear rate are essential for obtaining accurate Herschel-Bulkley parametrizations for the fiber suspensions using xanthan gum

as suspending liquid. When comparing the viscosity measurements to the laminar pipe friction pressure measurements, the narrow gap geometry seems to produce the better match. The friction pressure measurements for the non-Newtonian fiber suspensions were in excellent agreement with the theoretical friction factor prediction and the viscometer measurements even at Reynolds numbers up to approximately 1000. Future studies may assess whether the viscosity measurements are sensitive to wall roughness and whether the agreement between viscosity and friction pressure measurements also holds in larger pipe diameters, where particle confinement is reduced. Finally, the impact of PVA on the rheological behavior of conventional well cement slurries should be studied, along with the distribution of fibers in hardened cement plugs and annular cement sheaths.

References

1. R. M. Ahmed and N. E. Takach. Fiber Sweeps for Hole Cleaning. *SPE Drilling & Completion*, 24(04):564–573, 2009. SPE-113746-PA.
2. J. Mewis and N. J. Wagner. *Colloidal Suspension Rheology.* Cambridge University Press, 2013.
3. L. Pu, P. Xu, M. Xu, J. Song, and M. He. Effect of Fiber on Rheological Properties and Flow Behavior of Polymer Completion Fluids. *ACS Omega*, 6:17136–17148, 2021.
4. P. J. Krochak, J. A. Olson, and D. M. Martinez. Near-wall estimates of the concentration and orientation distribution of a semi-dilute rigid fibre suspension in Poiseuille flow. *J. Fluid Mech.*, 635:431–462, 2010.
5. D. Mezi, G. Ausias, S. G. Advani, and J. Férec. Fiber suspension in 2D nonhomogeneous flow: The effects of flow/fiber coupling for Newtonian and power-law suspending fluids. *Journal of Rheology*, 63(3):405–418, 2019.
6. R. J. Phillips, R. C. Armstrong, R. A. Brown, A. L. Graham, and J. R. Abbott. A constitutive equation for concentrated suspensions that accounts for shear-induced particle migration. *Physics of Fluids*, 4(1):30–40, 1992.
7. N. Xue, J. K. Nunes, and H. A. Stone. Shear-induced migration of confined flexible fibers. *Soft Matter*, 18:514–525, 2022.
8. V. N. Lima, H. J. Skadsem, K. Beltrán-Jiménez, R. Q. Velloso, and F. de A. Silva. On the early age mechanical properties, rheology and triaxial behavior of class G oil well cement paste considering polyvinyl alcohol microfiber as reinforcement. In preparation.
9. É. Lac and A. Parry. Non-Newtonian end-effects in standard oilfield rheometers. *Journal of Rheology*, 61(4):833–843, 2017.
10. H. J. Skadsem and A. Saasen. Concentric cylinder viscometer flows of Herschel-Bulkley fluids. *Appl. Rheol.*, 29(1):173–181, 2019.
11. K. Madlener, B. Frey, and H. K. Ciezki. Generalized Reynolds Number for Non-Newtonian Fluids. *Progress in Propulsion Physics*, 1:237–250, 2009.
12. R. J. Poole and B. S. Ridley. Development-Length Requirements for Fully Developed Laminar Pipe Flow of Inelastic Non-Newtonian Liquids. *Journal of Fluids Engineering*, 129(10):1281–1287, 2007.